Mapping Stanford Campus Elevation: A Sensor Fusion Approach

Erin Daly, Nolan Topper, Wei Lin Puah
Stanford University

1. INTRODUCTION

Modern smartphones are equipped with a variety of sensors, including GPS, accelerometers, and barometers, which allow them to function as convenient data logging devices. Apps such as Google's GNSSLogger and the Phyphox app can record this sensor data and export it for further analysis. While smartphone GPS provides latitude and longitude measurements accurate to approximately 1-5m, vertical altitude measurements are significantly less precise, often varying by 5-15m or more (Yun et al., 2022). Barometric pressure sensors can provide additional information about elevation, but readings are affected by weather conditions and require calibration (Matyja et al., 2024). To improve altitude estimates, sensor fusion techniques such as the Kalman filter can combine GPS and barometric data, leveraging the strengths of both sources (Yao & Huang, 2009). Despite their lower precision compared to professional GNSS surveying equipment, smartphones offer an accessible, low-cost way to map elevation changes. In this project, we aim to study elevation changes around the Stanford campus using smartphone sensors, Kalman filtering, and barometric data. Our goals are to evaluate the effectiveness and limitations of these methods and to quantify elevation changes relevant for campus activities such as biking. Understanding these elevation profiles can help students plan more efficient or less strenuous routes while demonstrating the practical potential of smartphone-based topographical mapping.

2. LITERATURE REVIEW

Researchers consistently find that combining barometric pressure data with GPS improves altitude estimation because the two sensors have complementary strengths: GPS provides an absolute vertical reference but with high noise and poor geometry, while barometers offer smooth, low-noise short-term altitude changes but suffer from drift and weather dependence. Ho et al. (2018) demonstrated this clearly for smartphones, showing that even low-cost phone barometers can significantly stabilize vertical readings and improve discrimination between roadway elevations (e.g., overpasses vs. underpasses). Their approach uses lightweight filtering to fuse GPS altitude with pressure-derived relative altitude, yielding practical accuracy gains in consumer navigation scenarios.

For systems requiring higher accuracy or robustness, more advanced fusion architectures appear in the literature. Kim and Sukkarieh (2003) showed that adding a barometric altimeter to an INS/GPS Kalman filter improves vertical observability and reduces drift during GPS outages in UAV flight tests. At the high-integrity end, Simonetti et al. (2024) developed a method to convert barometric pressure to precise geodetic altitude using meteorological data and formal error modeling, demonstrating that baro-derived altitude can safely augment GNSS for aviation. Together, these papers highlight that barometric measurements meaningfully enhance vertical positioning across domains—from consumer devices to UAV navigation to safety-critical aviation—when fused with GPS using appropriately modeled uncertainties.

Although the methods proposed by Kim and Sukkarieh (2003) and Simonetti et al. (2024) achieve higher accuracy, they involve considerably more complex processing pipelines and require extensive calibration. In contrast, our study focuses on a simpler fusion approach using only barometric and GPS measurements within a two-state Kalman filter framework. This allows us to systematically investigate the influence of individual parameters without the overhead of auxiliary sensors or external meteorological data, while still capturing the essential benefits of barometer–GPS integration.

3. METHOD FOR FILTERING

The altitude estimation problem in this project is based on a two–state linear Kalman filter, originally introduced by Kalman in his seminal paper (Kalman, 1960). The modern Bayesian interpretation of the filter, along with the full probabilistic derivation, follows the exposition of Simon (2006), while the classical optimal–filtering framework is presented in detail by Anderson and Moore (1979). For an accessible engineering tutorial, we also refer to the survey of Welch and Bishop (2006). The filter that was developed was a recursive discrete-time Kalman Filter (KF) to fuse high-frequency Global Positioning System (GPS) data with high-precision barometric pressure readings. The filter operates on a *Predict-Update* cycle to estimate the vertical state vector $\mathbf{x}_k$ at each time step k:

$$\mathbf{x}_k = \begin{bmatrix} h_k \\ v_k \end{bmatrix} \tag{1}$$

where h_k is the absolute altitude (m) and v_k is the vertical velocity (m/s).

3.1 Time Update (Prediction Phase)

In the prediction phase, the filter projects the state forward using a Constant Velocity (CV) kinematic model. This corresponds to the physics assumption that momentum is conserved between sampling intervals Δt. The *a priori* state estimate $\hat{\mathbf{x}}_k^-$ is calculated as:

$$\hat{\mathbf{x}}_k^- = \mathbf{F}\hat{\mathbf{x}}_{k-1} + \mathbf{w}_k \tag{2}$$

The state transition matrix $\mathbf{F}$ applies Newtonian mechanics:

$$\mathbf{F} = \begin{bmatrix} 1 & \Delta t \\ 0 & 1 \end{bmatrix} \tag{3}$$

This operation effectively predicts the new altitude as $h_{new} = h_{old} + v_{old}\Delta t$.

To account for deviations from this ideal model (e.g., uneven terrain or gait changes), we introduce process noise $\mathbf{w}_k \sim \mathcal{N}(0, \mathbf{Q})$. The process noise covariance $\mathbf{Q}$ determines the system's "stiffness":

$$\mathbf{Q} = \begin{bmatrix} Q_{pos}\Delta t & 0 \\ 0 & Q_{vel}\Delta t \end{bmatrix} \tag{4}$$

We selected low values for Q_{pos} (0.01) and Q_{vel} (0.001) to imply high system inertia, forcing the filter to smooth out transient sensor errors.

3.2 Measurement Model

At each time step, the filter receives an observation vector $\mathbf{z}_k$ containing raw sensor data:

$$\mathbf{z}_k = \begin{bmatrix} z_{baro} \\ z_{gps} \end{bmatrix} = \mathbf{H}\mathbf{x}_k + \mathbf{v}_k \tag{5}$$

The observation matrix $\mathbf{H}$ maps the state space to the sensor space. Since both sensors observe altitude directly but do not measure velocity, $\mathbf{H}$ is defined as:

$$\mathbf{H} = \begin{bmatrix} 1 & 0 \\ 1 & 0 \end{bmatrix} \tag{6}$$

The measurement noise $\mathbf{v}_k$ is modeled by the covariance matrix $\mathbf{R}$, which was tuned based on sensor precision:

$$\mathbf{R} = \begin{bmatrix} \sigma_{baro}^2 & 0 \\ 0 & \sigma_{gps}^2 \end{bmatrix} = \begin{bmatrix} 2.0 & 0 \\ 0 & 5.0 \end{bmatrix} \tag{7}$$

3.3 Kalman Measurement Update

Following the classical derivation in (Anderson & Moore, 1979; Kalman, 1960), the filter proceeds in two steps:

Prediction

$$\hat{\mathbf{x}}_{k|k-1} = \mathbf{F}_k\hat{\mathbf{x}}_{k-1|k-1}, \qquad \mathbf{P}_{k|k-1} = \mathbf{F}_k\mathbf{P}_{k-1|k-1}\mathbf{F}_k^\top + \mathbf{Q}_k.$$

Update

$$\mathbf{S}_k = \mathbf{H}\mathbf{P}_{k|k-1}\mathbf{H}^\top + \mathbf{R}, \qquad \mathbf{K}_k = \mathbf{P}_{k|k-1}\mathbf{H}^\top \mathbf{S}_k^{-1},$$
$$\hat{\mathbf{x}}_{k|k} = \hat{\mathbf{x}}_{k|k-1} + \mathbf{K}_k \left(\mathbf{z}_k - \mathbf{H}\hat{\mathbf{x}}_{k|k-1}\right),$$
$$\mathbf{P}_{k|k} = (\mathbf{I} - \mathbf{K}_k\mathbf{H})\,\mathbf{P}_{k|k-1}.$$

These equations arise directly from minimizing the expected quadratic estimation error under linear Gaussian assumptions, as discussed in (Anderson & Moore, 1979; Simon, 2006). Under our tuning parameters ($\sigma^2_{gps} > \sigma^2_{baro}$), the gain matrix $\mathbf{K}$ converges to a steady state that assigns significantly higher weight to the barometric pressure for short-term updates, while utilizing the GPS data to bound long-term drift.

3.4 Initialization and Bias Correction

To align the relative pressure changes with absolute geodetic altitude, we implemented a dynamic calibration routine. The Sea Level Pressure reference (P_0) was back-calculated by averaging the first 60 seconds of GPS data, ensuring the barometric altitude:

$$h_{baro} = 44330 \left(1 - \left(\frac{P}{P_0}\right)^{\frac{1}{5.255}}\right) \tag{8}$$

was initialized to the local absolute frame. The result is a smoothed altitude trajectory and an estimate of vertical velocity that is dynamically consistent, sensor–fusion optimal, and less noisy than either raw data stream.

4. EXPERIMENTAL STUDIES AND RESULTS

4.1 Benchmark Study: Static Sensor Analysis

To characterize the noise profiles of our sensors before dynamic implementation, we conducted a stationary benchmark study. Data was collected using the Phyphox application at two known National Geodetic Survey (NGS) benchmarks on the Stanford campus: the disk at Building 310 (NOAA National Geodetic Survey, n.d.-b) and the disk at the Cantor Arts Center (NOAA National Geodetic Survey, n.d.-a). After identifying the benchmark disks at each site, stationary measurements of GPS and barometric pressure were recorded for a duration of 2.5 minutes while standing within 1 m distance adjacent to each benchmark. The smartphone, an iPhone 13 model, was held approximately 1 m above the ground with the screen facing towards the sky. Both sets of data were taken on the same day approximately 10 minutes apart.

The initial 30 seconds of data were removed to allow the sensors to stabilize and reduce transient effects. The remaining barometric pressure values were then converted to altitude using Equation (8). The results highlighted distinct characteristics for each sensor:

- **Building 310:** The datasheet orthometric height is 29.25m. The experimental mean altitude was recorded at 30.08m.
- **Cantor Arts Center:** The datasheet orthometric height is 24.11m. The experimental mean altitude was recorded at 25.64m.

As illustrated in the time-series plots (**Figure 1**), the GPS altitude measurements exhibited significant high-frequency fluctuation compared to the barometric-derived altitude. However, the barometer measurements, while smoother, demonstrated a consistent offset from the datasheet orthometric height. This offset is partly due to atmospheric conditions and weather effects, and also contributed by a difference between the height where the smartphone was held and the benchmark disk height. These observations highlighted the necessity of a calibration window (P_0 determination) at the beginning of any data collection run.

4.2 Repeatability Study: Hill Repeats

To evaluate the consistency of the filter and its ability to handle dynamic elevation changes, a repeatability test was performed on Constanzo Street. This location was chosen because of its significant gradient. The procedure involved six repeated climbs and descents (hill repeats) using GNSSLogger and Phyphox for iPhone. These GNSSLogger measurements gave us two sets of data: raw GPS altitude and Fused Location Provider (FLP) as shown in **Figure 2**. The FLP uses GPS data as well as other sensor readings such as cellular and Wi-Fi signals to get a more balanced measurement. This calcuation occurs on Google servers with unknown variables. The Phyphox barometer and GPS data were collected simultaneously (**Figure 3**). Phyphox

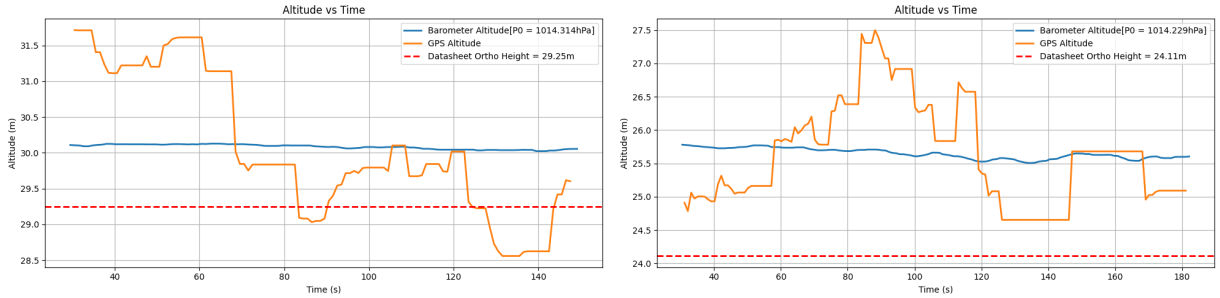

FIGURE 1: Static altitude measurements at Building 310 (left) and Cantor Arts Center (right). The blue line represents raw barometric altitude (smooth but offset), and the orange line represents raw GPS altitude. The red dashed line represents the benchmark data.

is collected using an iOS device and per iOS standards location data from the mobile and Wi-Fi networks are incorporated (Phyphox, 2025).

The raw GNSS altitude profile exhibited erratic spikes and ”jumps,” making it difficult to discern the distinct peaks of the six repetitions. The FLP data gave us clean and precise altitude data, but loose positional data as well as some odd behavior–the graph seems to cut off data at a bottom range. In contrast to either of these methods, the Kalman filtered output produced a smooth, periodic wave pattern that accurately reflected the physical activity.

A notable finding during this study was the presence of sensor drift. During the duration of the experiment (approximately 700 seconds), a linear drift was observed in the barometric data, likely attributed to minor weather-induced pressure changes or temperature variations during the exertion. This suggests that while the Kalman filter effectively handles high-frequency noise, long-duration scans require weather-aware corrections. Another proposed idea would be to include the weather bias to the estimation parameter, which might balance the weather effects.

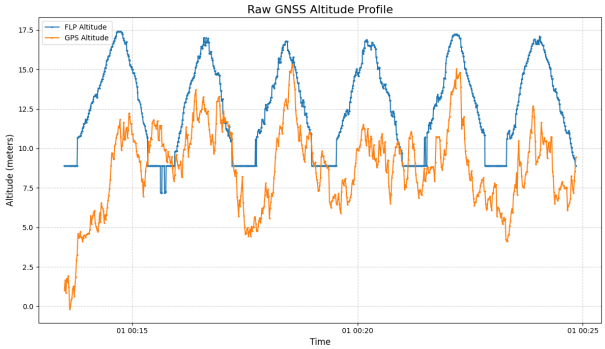

FIGURE 2: Altitude data from GNSSLogger. Orange line represents raw GPS, while blue line represents FLP data.

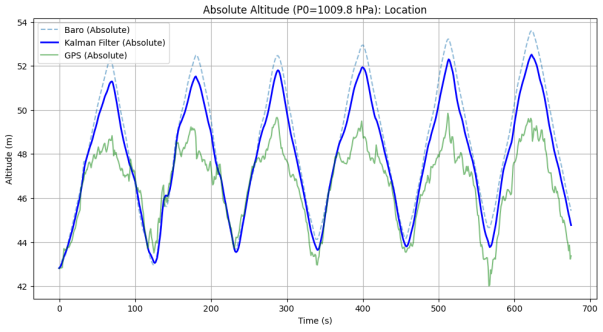

FIGURE 3: Graph showing raw altitude, barometric readouts, and Kalman filtered data. Data from Phyphox.

5. FILTER APPLICATION AND VALIDATION

To validate the sensor fusion algorithm in a real-world setting, we conducted a dynamic data collection run across the Stanford campus. This “local measurement” loop was designed to pass through varied terrain and intersect with our known benchmarks (Cantor Arts Center and Building 310) to allow for absolute accuracy verification.

5.1 Calibration Procedure

Correct initialization of barometric pressure is critical for accurate altitude estimation. As visualized by the yellow highlighted region in **Figure 5**, we implemented a specific calibration routine at the beginning of the data collection. The first 15 seconds of data were discarded to allow the sensors to stabilize. The average pressure over the subsequent 60-second window. This average was set as our reference pressure (P_0) for the barometric altitude formula for the remainder of the test.

5.2 Results and Benchmark Comparison

Figure 4 presents the results of the campus loop. The heatmap visualizes the Kalman Filtered absolute altitude over the 2D GPS path, showing a coherent elevation profile. The time-series plot in **Figure 5** demonstrates the filter's behavior: the blue Kalman estimate successfully rejects the high-frequency noise of the raw GPS (green line) while tracking the smoother trend of the barometer.

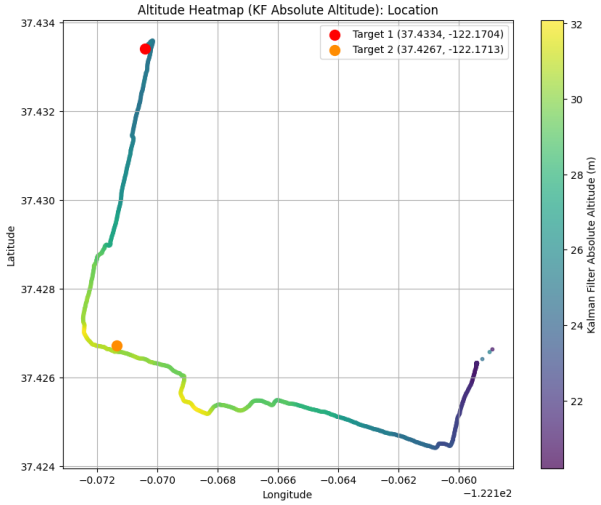

FIGURE 4: Altitude Heatmap (KF Absolute Altitude).

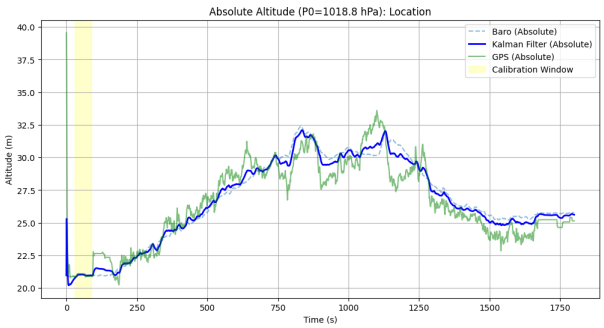

FIGURE 5: Altitude vs. Time (Yellow = Calibration).

Table 1 compares the altitude readings at our two checkpoint locations with the known data sheets of the National Geodetic Survey (NGS). The Kalman filter successfully fused the inputs to produce a stable estimate, though it remained subject to the initial offsets present in the raw sensor data.

Measurement Source	Cantor Arts Center (m)	Building 310 (m)
Benchmark (Truth)	**24.11**	**29.25**
GPS (Raw)	25.14	30.88
Barometer (Raw)	25.79	30.34
Kalman Filter	**25.67**	**30.31**

Table 1: Comparison of sensor outputs against benchmarks.

5.3 Residual Analysis

To quantitatively assess the model's performance, we analyzed the measurement residuals—the difference between the predicted state and the actual measurement. To ensure the Kalman filter was optimally estimating the state variables, the filter's internal parameters and the statistical properties of the measurement residuals were analyzed. This was done by manually breaking apart to isolate the specifc contribution of each sensor.

5.4 Filter Update and Convergence

The state update step is governed by the standard Kalman update equation, which fuses the prediction with the weighted innovations from both sensors:

$$x_{new} = x_{pred} + \mathbf{K}_{baro}(y_{baro}) + \mathbf{K}_{gps}(y_{gps}) \tag{9}$$

Where $\mathbf{K}$ represents the Kalman Gain, effectively serving as the weighting factor for each sensor based on its uncertainty.

As shown in **Figure 6**, the Kalman gains for both the barometer and GPS altitude rapidly converged to steady-state values within the first few seconds of the trial. The barometer weight settled at a significantly higher value (approx 0.16) compared

to the GPS weight (approx 0.06), reflecting the filter's reliance on the barometer's superior short-term precision over the noisy GPS signal.

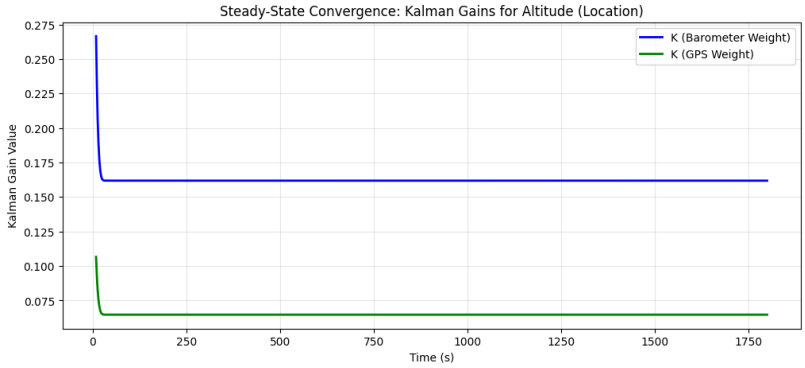

FIGURE 6: Steady-State Convergence of Kalman Gains.

Barometer Residuals

The barometer residuals (**Figure 7**) displayed a compact error distribution with a mean near zero (Mean: 0.095). The Histogram and Q-Q plot closely tracked the theoretical normal distribution line, confirming that the barometric noise is well-modeled as Gaussian white noise for this application.

GPS Residuals

The GPS residuals (**Figure 8**) exhibited a wider variance and a slight negative bias (Mean: -0.208). While the Q-Q plot shows some deviation in the tails, the distribution is sufficiently normal to justify the linear Gaussian assumption used in the standard Kalman Filter. The time-series analysis of GPS residuals confirms the sensor's instability in the vertical axis, justifying the tuning parameters chosen for the R matrix ($\sigma^2_{baro} = 2.0$ vs $\sigma^2_{gps} = 5.0$), which heavily penalizes GPS variance in the update step.

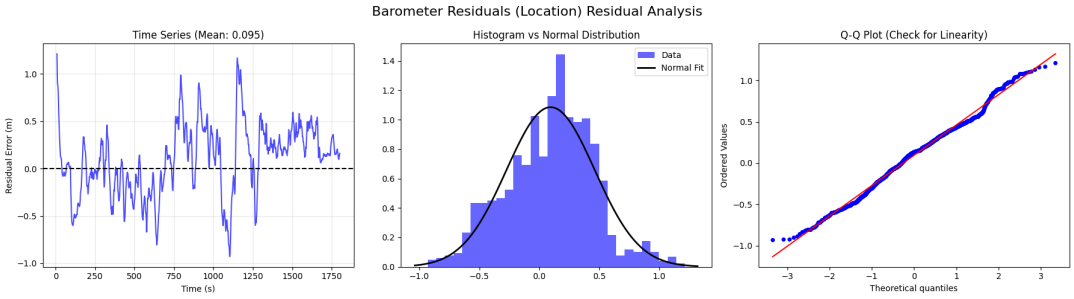

FIGURE 7: Barometer Residual Analysis.

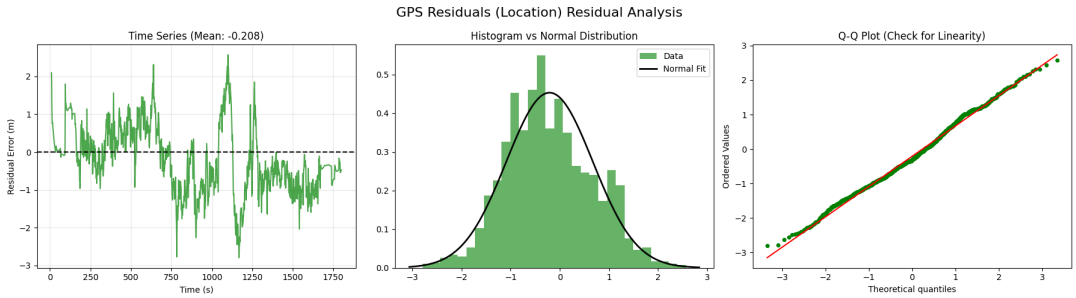

FIGURE 8: GPS Residual Analysis.

Measurement Source	**Measurement Noise Covariance (R)**	**Observed Characteristics**
Barometer	$\sigma^2 = 2.0$	Low noise, subject to drift
GPS	$\sigma^2 = 5.0$	High noise, bounded absolute error

Table 2: Tuning parameters derived from residual analysis.

5.5 Campus Elevation Mapping

The final experimental phase involved a full-campus loop to generate a 2D elevation heatmap. The route covered varied terrain to test the filter's performance over a larger spatial domain. We intended to gather FLP, GPS and pressure data to create the heatmap, but we had some technical troubles with Google Play Services. We were only able to collect GPS data from Garmin, and they filter their own data and correct for elevation.

The resulting heatmap (**Figure 9**) from the Garmin data visualizes an elevation range of approximately 32 meters across the campus. The raw GPS path exhibited "jitter" in both the horizontal and vertical planes. The Garmin data successfully smoothed these fluctuations, resulting in a coherent elevation map suitable for the proposed bike route planning application. This is a result similar to what we would expect our Kalman filter to provide, but would need to recollect data to compare.

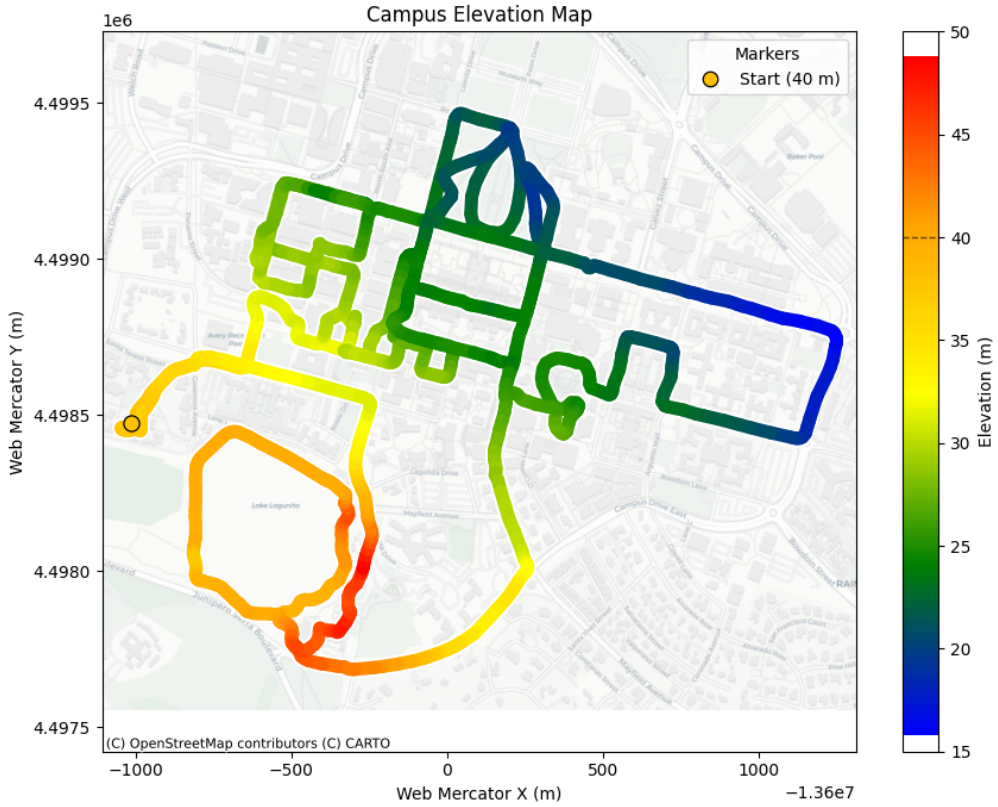

FIGURE 9: Barometer Residual Analysis.

6. DISCUSSION

The implementation of the Kalman Filter demonstrated a successful fusion of complementary sensor data, validating the hypothesis that combining barometric pressure with GNSS improves vertical estimation accuracy. By leveraging the low-noise characteristics of the barometer for short-term updates and the absolute positioning of the GNSS to bound long-term drift, the filter produced an elevation profile significantly smoother than raw GNSS data.

6.1 Filter Performance and Convergence

The system state covariance matrix (P) and Kalman Gain (K) successfully converged to steady-state values during dynamic testing. As shown in the residual analysis, the filter quickly adapted to the measurement noise covariances set in the R matrix ($R_{baro} = 2.0$, $R_{gps} = 5.0$). The steady-state Kalman gain favored the barometer for high-frequency updates, effectively acting as a low-pass filter against the erratic vertical jumps inherent to consumer-grade GPS receivers.

6.2 Limitations and Environmental Factors

While the fusion algorithm improved general stability, two primary limitations were identified during the experimental trials:

1. **Weather Sensitivity and Drift:** The barometer's reliance on atmospheric pressure makes it susceptible to environmental changes. During the repeatability study, a linear drift was observed in the raw barometric data over the 700-second duration. Because the current model assumes a constant sea-level pressure (P_0) derived from the initial calibration window, any change in local weather (temperature or humidity) manifests as a false change in altitude.

2. **Initialization Sensitivity:** The accuracy of the absolute altitude estimates is highly dependent on the initial calibration phase. As noted in the benchmark study, determining the correct reference pressure (P_0) requires a stationary period

to establish a baseline. Errors in this initial ”calibration window” propagate as a constant offset throughout the entire dataset.

6.3 Implications for Route Planning

Despite the drift limitations, the resulting elevation map provides a sufficient level of detail for the project's primary motivation: bike route planning. The filter successfully discriminated between the significant elevation changes of the campus hills without the confusing ”noise” that often characterizes raw GPS tracks. The smoothed profiles allow for a realistic calculation of total elevation gain, a metric that is typically grossly overestimated by raw, noisy GPS data.

7. TEAM MEMBER CONTRIBUTIONS

Erin	Nolan	Wei Lin
• Repeatability study data analysis • Kalman filter implementation, tuning, and processing • Presentation Slides • Project Report	• Repeatability study data collection • Heatmap data collection • Heatmap data analysis • Presentation Slides • Project Report	• Benchmark study data collection • Benchmark study data analysis • Presentation Slides • Project Report

Table 3: Distribution of project responsibilities among team members.

8. CONCLUSION

This project successfully implemented and validated a sensor fusion algorithm for mapping campus elevation. Our experimental results support the following conclusions:

- **Sensor Characteristics:** The GPS altitude signal was confirmed to be noisy and unstable in the vertical axis, suffering from a low sampling rate that missed fine terrain details. In contrast, the barometric altimeter provided a significantly smoother signal with a higher sampling rate.
- **Drift and Calibration:** While smoother, the barometer was highly sensitive to initial pressure assumptions (P_0) and exhibited drift due to changing weather conditions (temperature and pressure shifts) over the duration of the collection.
- **Fusion Success:** The Kalman filter successfully fused the complementary strengths of both sensors. By using the GPS to bound the absolute error and the barometer to smooth the high-frequency transitions, the filter produced a cleaner, more stable altitude estimate than either sensor could achieve individually.

As seen in **Figure 10**, the sensor fusion significantly improves the vertical profile. While the FLP shows significant improvement in the vertical direction estimate; there are errors induced by the added sensors (**Figure 10a**), over complicating the system resulting drift in position. Conversely, the GPS signal shown in **Figure 10b** is highly unstable and an inaccurate measurements of the altitude. The final Kalman filter output, visualized in **Figure 10c**, successfully combines the stability of the pressure data with the absolute accuracy of the GPS. Creating a very precise measurement.

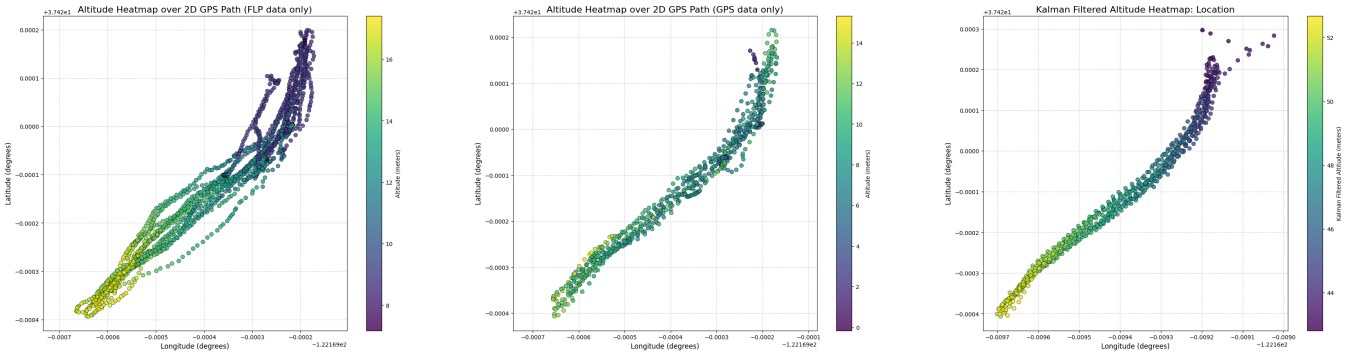

(a) FLP Data(Drift) **(b)** GPS Only (Noisy/Unstable) **(c)** Kalman Filtered (Stable)

FIGURE 10: Comparison of altitude heatmaps showing the stabilizing effect of the Kalman Filter.

9. FUTURE WORK

Future improvements to the elevation mapping system will focus on mitigating environmental drift, improving the model, and enhancing sensor precision. To address the barometric instability observed during long-duration trials, future iterations should integrate real-time meteorological data—specifically temperature and humidity gradients—to dynamically correct pressure readings rather than relying on a static initial calibration.

Additionally, the absolute vertical accuracy of the system could be significantly improved by incorporating Differential GPS (DGPS) or Real-Time Kinematic (RTK) processing, which would reduce the baseline noise of the GNSS measurements. Finally, fusing vertical acceleration data from the smartphone's Inertial Measurement Unit (IMU) would provide a high-rate control input to the Kalman filter, allowing the system to better distinguish between true physical elevation changes and sensor drift.

Finally, in this project, the Kalman filter was applied to data collected using the Phyphox app, which provides orthometric height, and this was verified by comparing the measurements against the surveyed benchmark datasheets. However, a systematic offset was observed when comparing elevations from the GNSSLogger app, which outputs ellipsoidal height. In future work, if data from multiple applications are to be fused, it will be essential to ensure that all height measurements are referenced consistently by accounting for the geoid height changes so that fused altitude estimates remain accurate and comparable across sources.

References

Anderson, B. D. O., & Moore, J. B. (1979). *Optimal filtering*. Prentice Hall.

Ho, P.-F., Hsu, C.-C., Chen, J.-C., & Zhang, T. (2018). Using barometer on smartphones to improve gps navigation altitude accuracy [Available in ACM Digital Library]. *ACM Poster and Short Paper*.

Kalman, R. E. (1960). A new approach to linear filtering and prediction problems. *Transactions of the ASME–Journal of Basic Engineering*, *82*(1), 35–45.

Kim, J. H., & Sukkarieh, S. (2003). A baro-altimeter augmented ins/gps navigation system for an uninhabited aerial vehicle [See also related publications by the authors]. *Proc. International Symposium on Satellite Navigation Technology*.

Matyja, T., Stanik, Z., & Kubik, A. (2024). Automatic correction of barometric altimeters using additional air temperature and humidity measurements. *GPS Solutions*, *28*. https://doi.org/10.1007/s10291-023-01582-7

NOAA National Geodetic Survey. (n.d.-a). Ngs datasheet for mark: Ht1343 (cantor arts center) [Accessed 2025].

NOAA National Geodetic Survey. (n.d.-b). Ngs datasheet for mark: Ht1345 (building 310) [Accessed 2025].

Phyphox. (2025). *Location (gps) experiment* [Accessed: 2025-11-29]. https://phyphox.org/experiment/location-gps/

Simon, D. (2006). *Optimal state estimation: Kalman, h infinity, and nonlinear approaches*. Wiley.

Simonetti, M., et al. (2024). Geodetic altitude from barometer and weather data for gnss [Includes conversion methods, error/threat models, and flight-test validation]. *ION Navigation*, *71*(2).

Welch, G., & Bishop, G. (2006). *An introduction to the kalman filter* (tech. rep. No. TR 95-041) (Updated version of 1995 report). University of North Carolina at Chapel Hill.

Yao, Z.-G., & Huang, R. (2009). Data fusion algorithm of baro/gps based on delta-altitude [IEEE conference paper]. *Proceedings of YC-ICT '09 (Information, Computing and Telecommunication Conference)*, 522–525. https://ieeexplore.ieee.org/document/5382443

Yun, J., Lim, C., & Park, B. (2022). Inherent limitations of smartphone gnss positioning and effective methods to increase the accuracy utilizing dual-frequency measurements. *Sensors*, *22*(24), 9879. https://doi.org/10.3390/s22249879

10. APPENDIX

10.1 Benchmark Study

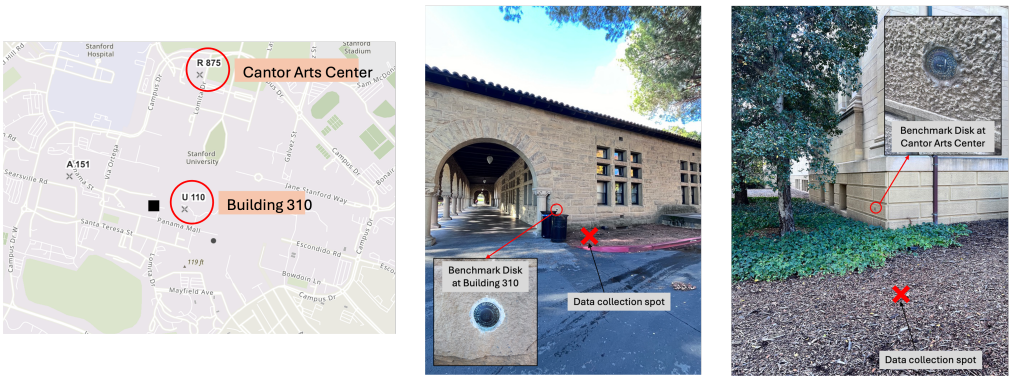

FIGURE 11: Benchmark and data collection locations.

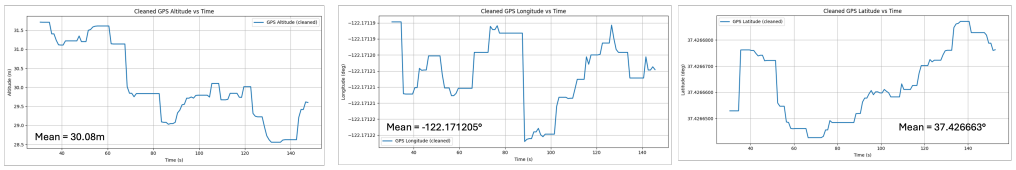

FIGURE 12: GPS location plot for Building 310.

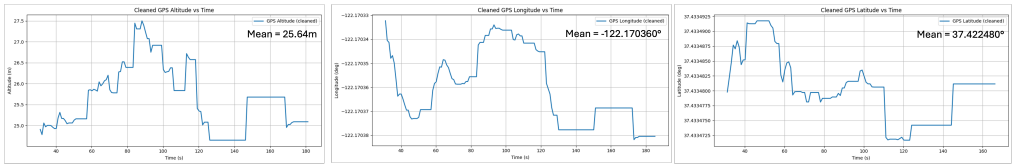

FIGURE 13: GPS location plot for Cantor Arts Center.

10.2 Repeatability Study

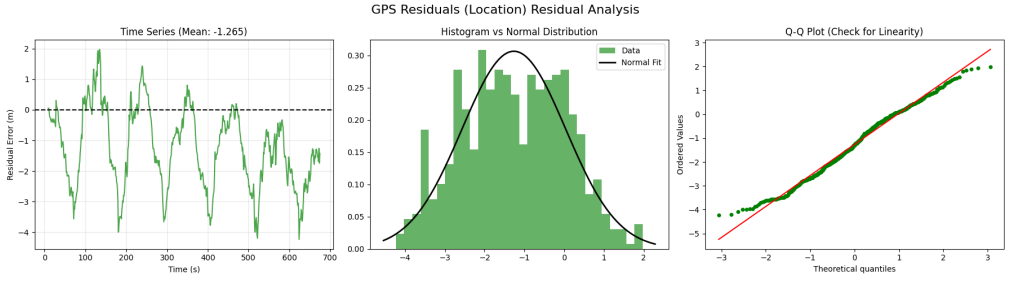

FIGURE 14: Residuals from the GPS data for the hill repeats.

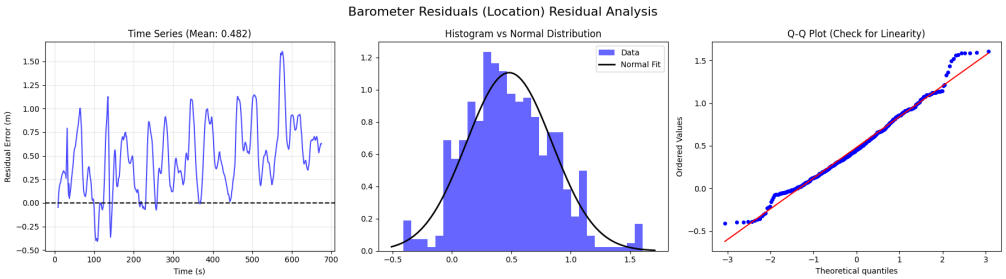

FIGURE 15: Residuals from barometer data for hill repeats

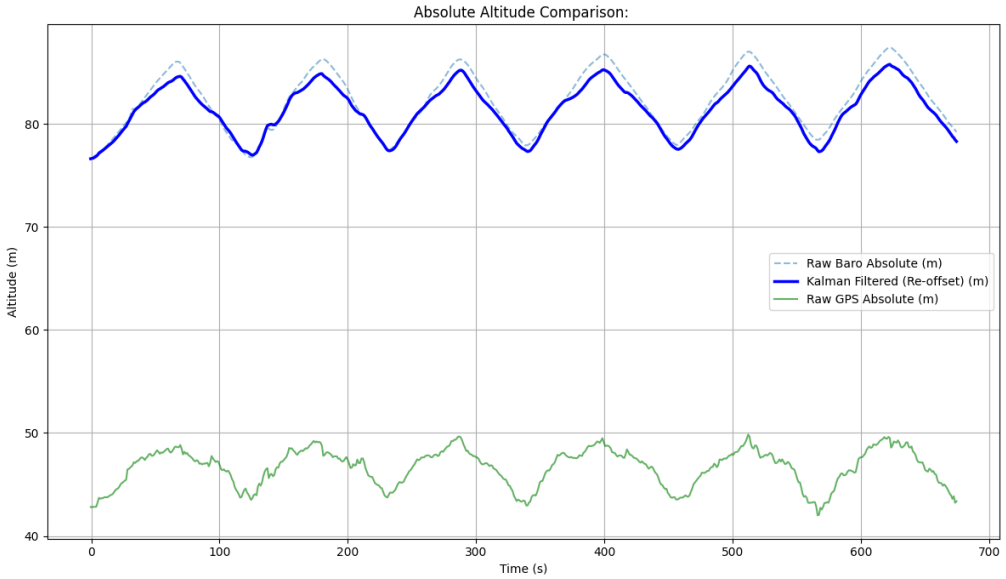

FIGURE 16: Absolute altitude comparison for GPS and barometer from the repeatability study.